Rock mapping of glaciated areas by satellite image processing

FRANCESCO SALVINI, ROBERTO DELLA MAGGIORE, LUCIANO FORTUNATI, and FRANCESCO MAZZARINI

A model is presented that performs spectral deicing of mixed pixels in satellite images of glaciated areas. The model was tested in Northern Victoria Land, Antarctica. For this region we assumed that pixels could be grouped in two broad categories representing pure ice and pure rock. Naturally mixed ice and rock pixels are present in satellite images; these were recomputed to separate the spectral component related to the rock fraction. We used Landsat TM images as input data and aerial photographs, maps and field surveys as reference data. By making use of sample populations of pixels corresponding to pure ice and to pure rock groundels (i.e. ground elements, the ground portions corresponding to each pixel), we detected the linear correlation between pairs of bands and selected the two most suitable bands. For every pixel falling between the correlation lines of the two categories, the rock fraction in the corresponding groundel was computed. This fractional value was then used to perform the automatic deicing process with which the DNs of the selected mixed pixels were recomputed. In the utilised Antarctic image, this process increases about 2.7 times the number of pixels in the pure rock category, allowing the production of enhanced images and, as a side product, a thematic map of rock percentage in the groundels.

F. Salvini and F. Mazzarini, Department of Earth Science, University of Pisa, Via S. Maria 53, I-56126 Pisa, Italy; R. della Maggiore and L. Fortunati, CNR (National Research Council), Institute CNUCE, Via S. Maria 36, I-56126 Pisa, Italy.

Introduction

The analysis of satellite images of polar areas is useful in enabling us to study glaciers and ice-shelf movements, prepare and tune topographic maps (Borfecchia & Frezzotti 1991) and perform geologic analyses of the tectonics (Fortunati et al. 1991) and morphotectonics of very large areas (Lucchitta et al. 1987, 1989; Bianchi et al. 1990, 1991).

The aim of our study was to produce enhanced images for further geologic research in Antarctic areas. We set up an algorithm to enhance the amount of information relating to the rocks in Landsat TM images.

The study area

The investigated area is Terra Nova Bay, located in Northern Victoria Land, a part of the Trans-antarctic Mountains (Antarctica). The area (Fig. 1) is delimited by the David Glacier to the South and the Aviator Glacier to the North and extends from the coast to the Southern Cross Mountains inland.

The glaciers are one of the main morphological features of this region (Orombelli 1989); they strike NW-SE and, near the coastline, rotate to N-S trend.

The geology of the area is characterised by the occurrence of a deformed polymetamorphic and igneous pre-to early paleozoic basement unconformably overlaid by sedimentary and volcanic covers (Carmignani et al. 1989a, b; Ganovex Team 1987; Giudice et al. 1991a, b; Kleinschmidt et al. 1984). The basement is cut by a regional peneplain over which the Permo-Triassic continental sediments of the Beacon Supergroup deposited. The Jurassic volcanic products of the Ferrar Group lie above these. Tertiary and Quaternary subaerial volcanic deposits overlay the described sequences (Gair et al. 1969).

We used satellite image data obtained from Landsat TM (acquisition date: 19/1/90, WRS: 062–113, scene id: 4274220412, bands: 1, 2, 3, 4, 5, 6, 7).

The model

In the satellite images of glaciated areas the pixels belong to many spectral classes, such as different lithologies, morains, blue ice, white ice, snow and water. Obviously the illumination conditions influence the amount of reflected e.m. energy for
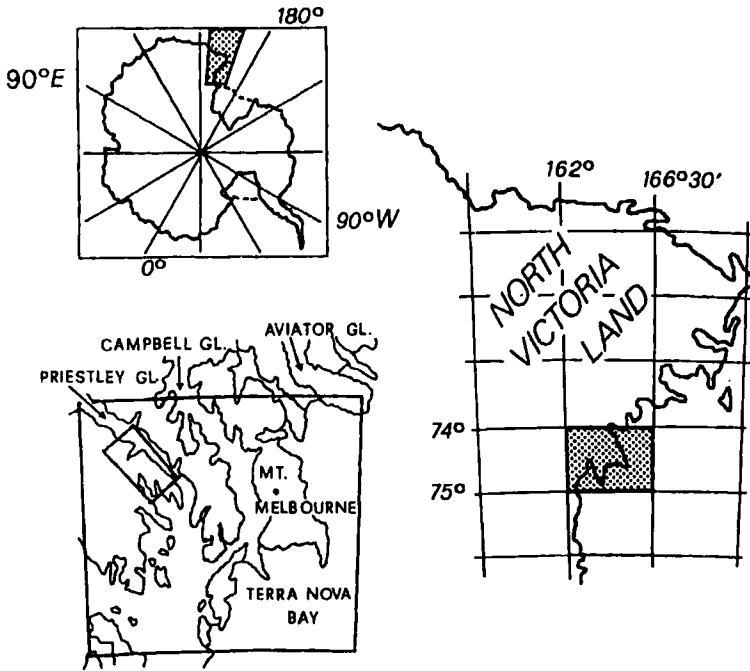
Fig. 1. Location map (modified after Giudice et al. 1991). The box within the detailed map represents the area of images in Fig. 7.

each of these classes. In this paper we assume, as first order approximation, that the pixels in the analysed image can be grouped into two main supercategories: Ice and Rock. The Ice and Rock supercategories (in the following referred as categories) are sharply and well defined spectrally and separate (diagrams of Fig. 4).

We assume that the pixel information in the image is linked to the ratio between rock extension and ice extension in the groundel (we define the groundel as the ground-element, i.e. the ground area corresponding to each pixel of a remotely sensed image). In this broad exemplification, there are pixels representing 100% rock groundels, pixels representing 100% ice groundels and mixed pixels (Wadge & Quarmby 1988) representing groundels where both the two types of outcrop (rock and ice) are present. We focused our attention on the features of the groundels represented by mixed pixels. We assumed that each pixel value (Digital Number, DN) can be considered a linear combination of the reflectance of the objects present in the groundel; consequently we can state the following relation:

$$P_\lambda = i_\lambda * (f*R_{r,\lambda} + (1 - f)*R_{i,\lambda}) + C_\lambda \qquad (1)$$

where:
P_λ is the DN for band λ;

i_λ is a factor proportional to the conditions of illumination of the groundel for band λ;

f is the fraction of outcropping rock in the groundel;

$R_{r,\lambda}$ is a factor proportional to mean rock category reflectance for band λ;

$R_{i,\lambda}$ is a factor proportional to mean ice category reflectance for band λ;

C_λ is a term that is proportional to the toe of the characteristic curve of the sensor for band λ.

The category reflectances are represented by mean values as a consequence of variability in the response of different types of rock and ice and as a consequence of the conditions of illumination. Nevertheless the ice category is always spectrally separate from the rock category (see again diagrams of Fig. 4).

Method

The process flow

Fig. 2 shows the global process in which two main flows are present: one is related to the evaluating operations to be performed propedeutically on test area samples, the other is related to the final production of enhanced and thematic images. The
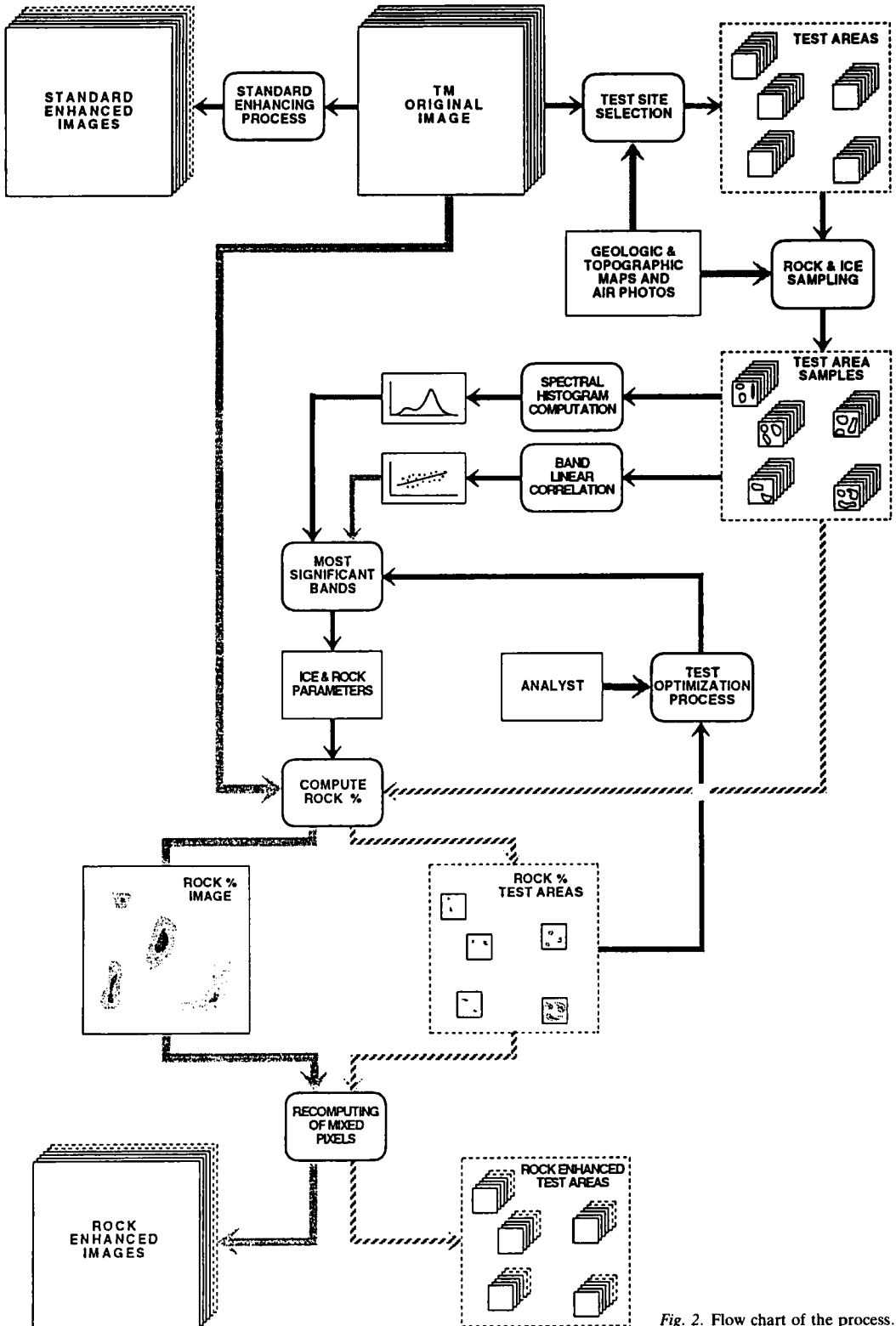
Fig. 2. Flow chart of the process.

input, output and intermediate data (including tuning performed by the analyst) are identified with quad boxes; the processing functions are performed in the rounded corner blocks. The logical flow of operations is made evident by using different patterns for the arrows which connect the blocks. Black arrows represent the tuning process; the light gray thick arrows show the final process and the oblique pattern arrows relate to the test process. The dark gray arrows represent the external control and the interactive process by the analyst.

Category discrimination

In the whole satellite scene 22 test areas were selected, each one with dimensions of 512 × 512 pixels. The total surface covered by the 22 test areas was about 14% of the whole Landsat TM scene. In each test area we selected homogeneous samples of pixels that represent the variability of

the two categories, rock and ice, related to the end members of the illumination conditions: lighted rock ($PM_{il,\lambda}$), shadowed rock ($PM_{rs,\lambda}$), lighted ice ($PM_{il,\lambda}$) and shadowed ice ($PM_{is,\lambda}$) subcategories. The collected samples were then validated as belonging to the assigned subcategory by making use of aerial photographs, maps (Carmignani et al. 1989a, b; Ganovex Team 1987; Giudice et al. 1991a, b), and field surveys (1986/87 PNRA Party). For each test area we computed the histograms of the selected samples and then evaluated the mean values and the standard deviations of the four subcategories for each spectral band. These parameters were obtained by regressions of multiple gaussian curves, according to the methodologies in Wise et al. (1985). Finally, we evaluated the global mean and standard deviation values of these statistical parameters. The results are listed in Table 1 (equal weight was assumed for each test area) and Table 2 (weighted means are based on the number of pixels for each sub-

Table 1. Mean values and standard deviations of test areas.

	Band 1	Band 2	Band 3	Band 4	Band 5	Band 6	Band 7
PM_{il}	254.99	188.73	223.43	172.26	31.99	55.38	17.41
σ	0.23	32.24	21.20	38.19	8.84	4.96	4.74
PM_{rl}	166.22	77.50	99.67	73.48	61.29	75.38	40.17
σ	43.61	31.34	40.92	30.86	20.10	9.05	13.80
PM_{is}	184.67	67.80	73.34	44.92	10.93	49.22	6.92
σ	35.17	23.71	31.54	22.30	5.38	5.32	3.36
PM_{rs}	122.90	42.99	45.37	27.98	19.14	58.74	12.63
σ	31.22	14.67	19.45	14.25	13.10	7.71	8.51

Table 2. Weighted mean values and standard deviations of test areas.

	Band 1	Band 2	Band 3	Band 4	Band 5	Band 6	Band 7
PM^w_{il}	223.06	161.53	191.97	145.65	26.45	48.32	14.47
σ	0.30	27.30	18.17	32.96	7.81	4.06	4.23
PM^w_{is}	149.96	68.20	88.16	65.16	58.48	69.80	38.84
σ	39.97	26.85	35.69	26.54	19.52	8.11	13.15
PM^w_{rl}	156.41	53.32	54.89	32.29	7.98	45.50	5.27
σ	29.47	17.96	24.12	17.50	4.28	5.11	2.73
PM^w_{rs}	111.59	38.15	39.37	24.05	15.70	53.05	10.41
σ	27.55	12.87	16.67	12.69	12.59	7.38	8.13

Table 3. Values of normalized parameters for the choice of the bands.

	Band 1	Band 2	Band 3	Band 4	Band 5	Band 6	Band 7
PM_{il}/PM_{rl}	1.530	2.430	2.240	2.340	0.520	0.730	0.430
PM_{is}/PM_{rs}	1.500	1.580	1.580	1.530	0.550	0.840	0.550
KI	0.010	0.212	0.173	0.209	−0.028	−0.070	−0.122
PM^w_{il}/PM^w_{rl}	1.490	2.370	2.180	2.230	0.450	0.690	0.370
PM^w_{is}/PM^w_{rs}	1.400	1.400	1.390	1.340	0.510	0.860	0.510
KI^w	0.031	0.257	0.221	0.249	−0.062	−0.120	−0.159

Rock Samples (Original)   **Ice Samples (Original)**

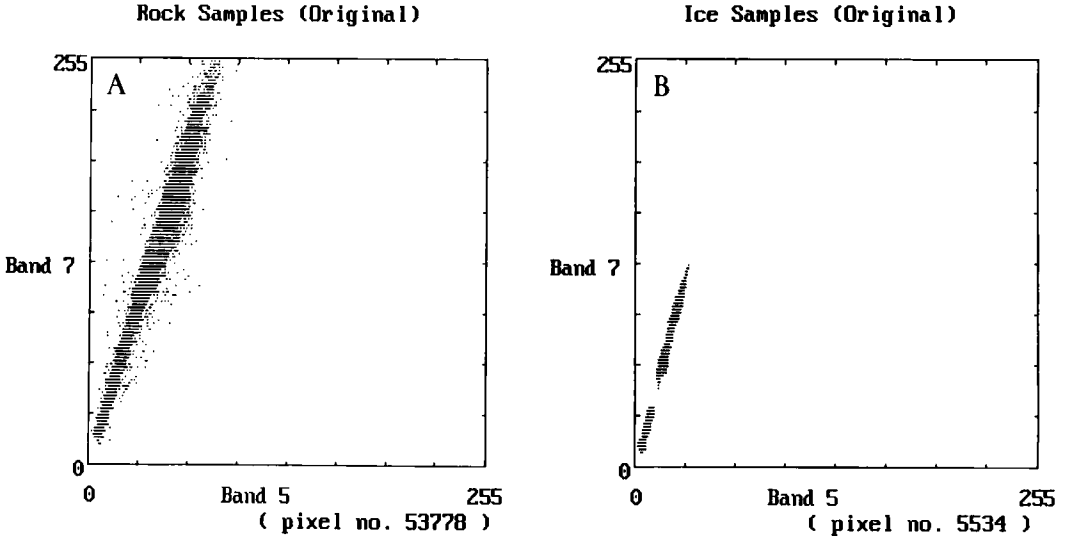*Fig. 3.* Scatterograms of original DNs of rock (A) and ice (B) samples for the 5,7 TM bands combination; note the strong correlation between the two categories.

category). In order to select the two most suitable bands to discriminate the categories, we defined the normalised parameter Kl as:

$$Kl = \{[(PM_{il,\lambda}/PM_{rl,\lambda}) - (PM_{is,\lambda}/PM_{rs,\lambda})]/$$

$$[(PM_{il,\lambda}/PM_{rl,\lambda}) + (PM_{is,\lambda}/PM_{rs,\lambda})]\}$$

Table 3 shows the computed values of the Kl and Kl^w (weighted) parameters: the smaller the Kl the more suitable the band. The Kl parameter doesn't seem to be affected by the method used to obtain the mean values. According to the ascending order of the Kl values, the order of the most suitable bands is: 1, 5, 6, 7, 3, 4, 2. Other factors should be considered: band 1 is affected by the haze and contains too many oversaturated pixels; band 5 seems to be good and we chose it as the first band; band 6 has insufficient geometric resolution; we prepared scatterograms for bands 7 and 5 (Fig. 3), and found that the correlation lines of the two categories are too similar; band 3 and band 5 show the most favorable scatterograms (Fig. 4). The selected bands were thus band 5 and band 3.

The enhancement process

Our aim was to produce enhanced image extracting rock information from mixed pixels in order to get enhanced images which best show

the original spectra of the various outcropping lithologies (Bierwirth 1990). We noted that if a mixed groundel was composed of 100% rock (i.e. f = 1) the value of its corresponding pixel would have on a reasonable approximation a linear relationship with the mean reflectance of rock category (for band λ) plus a scale factor (C_λ).

Computation of rock fraction, f

For each TM band λ and each category c we can approximate the relationship between the value of a pixel and the electro-magnetic (e.m.) characteristics of the corresponding groundel:

$$P_{c,\lambda} = i_\lambda * R_{c,\lambda} + C_\lambda \qquad (2)$$

where:
c category parameter, i.e. rock or ice;
$P_{c,\lambda}$ is the DN of a pixel corresponding to a groundel of category c for band λ;
$R_{c,\lambda}$ is a factor that is proportional to the mean reflectance of category c for band λ and takes into account the TM sensor versus incident e.m. energy conversion factor (the slope of the characteristic curve of the sensor).

We consider the diagram in the correlation space (DN$_{\lambda 1}$,DN$_{\lambda 2}$ i.e. scatterogram) for each category c and for any two TM bands λ_1,λ_2.

To study the ratio between $P_{c,\lambda 1}$ and $P_{c,\lambda 2}$ in the two λ_1,λ_2 bands and for objects of category c, we

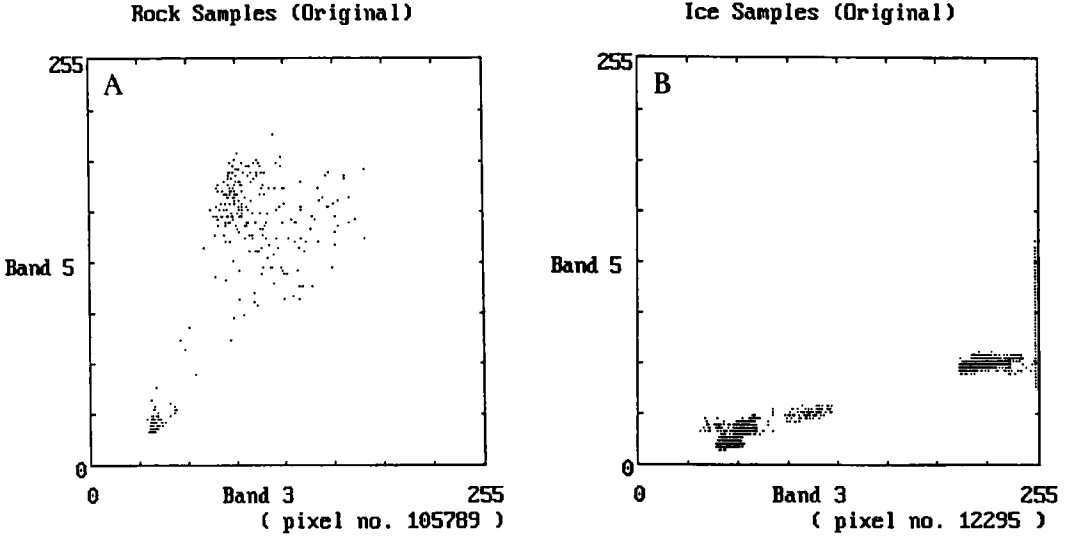**Rock Samples (Original)**   **Ice Samples (Original)**

Fig. 4. Scatterograms of original DNs of rock (A) and ice (B) samples for the 5,3 TM bands combination; note the differences between the two categories.

analyse the ratio between the two corresponding equations (2); we considered that for a given condition of illumination the ratio $i_{\lambda 1}/i_{\lambda 2} = I_{\lambda 1,\lambda 2}$ can be approximatively considered constant (see diagrams, Figs. 3 and 4); so we obtain:

$$(P_{c,\lambda 1} - C_{\lambda 1})/(P_{c,\lambda 2} - C_{\lambda 2}) = I_{\lambda 1,\lambda 2}*(R_{c,\lambda 1}/R_{c,\lambda 2})$$

Reducing the ratios and solving for $P_{c,\lambda 1}$, the resulting equation represents a straight line in the correlation space $(DN_{\lambda 1},DN_{\lambda 2})$:

$$P_{c,\lambda 1} = m_{c,\lambda 1,\lambda 2}*P_{c,\lambda 2} + k_{c,\lambda 1,\lambda 2}$$

with slope and intercept respectively:

$$m_{c,\lambda 1,\lambda 2} = I_{\lambda 1,\lambda 2}*(R_{c,\lambda 1}/R_{c,\lambda 2})$$

$$k_{c,\lambda 1,\lambda 2} = C_{\lambda 1} - \{I_{\lambda 1,\lambda 2}*(R_{c,\lambda 1}/R_{c,\lambda 2})\}*C_{\lambda 2}$$

Obviously this line will have different parameters depending on the choice of the pair of bands and on the category of objects.

As above mentioned we selected bands 5 and 3 as the most significant combination of bands for our identification purposes. We computed the parameters of the straight correlation lines of the rock category and of the ice category through selected samples. The m and k parameters for each category were obtained by linear regressions of sampled pixels which fall in the linear interval of the correlation diagram. This interval was visually identified in the diagram (Fig. 5). The two

resulting equations are:

$$P_{r,3} = m_r*P_{r,5} + k_r; \ P_{i,3} = m_i*P_{i,5} + k_i \quad (3)$$

Pixels representing groundels with mixed rock and ice fall in the correlation space $(DN_{\lambda 1},DN_{\lambda 2})$ between the two straight lines. We now consider the distance of one of these pixels in the correlation space from the line representing ice and normalise it by dividing its value by the sum of the distances from the two lines (Fig. 6). By indicating these distances with d_r and d_i, we can express the normalised distance of each pixel from the ice line as:

$$f = d_i/(d_r + d_i) \quad (4)$$

We assume that f is a good approximation of the percentage of outcropping rock in the groundel (rock percentage or fraction).

We computed the distances d_r and d_i as:

$$d_r = ABS\{(P_3 - m_r*P_5 - k_r)/((m^2_r + 1)^{1/2})\}$$
$$d_i = ABS\{(P_3 - m_i*P_5 - k_r)/((m^2_i + 1)^{1/2})\}$$

Mixed pixels recomputation

With reference to our model and to equation (2), and in order to compute the new value of each mixed pixel as if it were composed of 100% rock, we need to compute the values $i_\lambda*R_{r,\lambda}$ and C_λ.

Evaluating Equation (1) and dividing by $i_\lambda*R_{r,\lambda}$
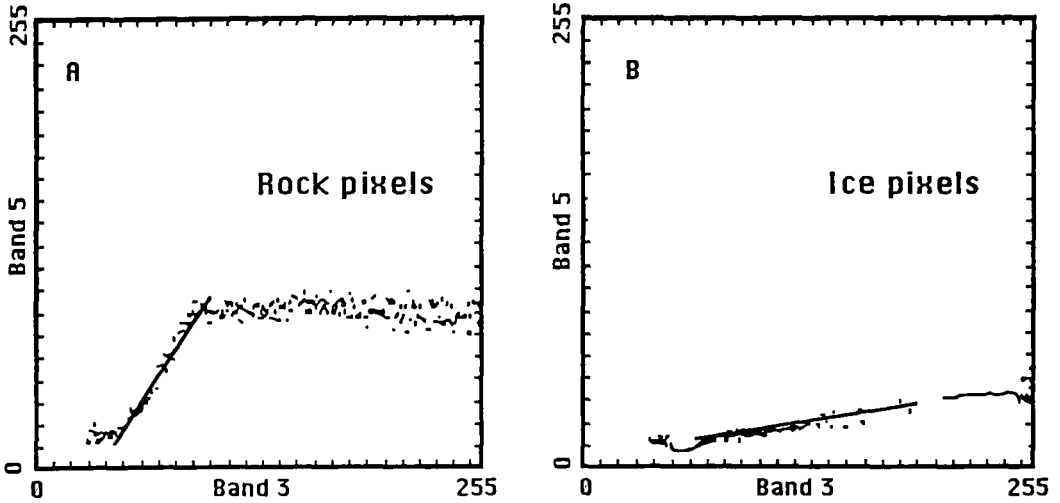
Fig. 5. Linear regression of total rock (A) and ice (B) samples. The straight segments show the computed lines and the considered ranges.

we obtain:

$$P_\lambda/(i_\lambda{}^*R_{r,\lambda})$$
$$= f + (1 - f)^*(R_{i,\lambda}/R_{r,\lambda}) + (C_\lambda/(i_\lambda{}^*R_{r,\lambda}))$$

By indicating with $S_\lambda = R_{i,\lambda}/R_{r,\lambda}$ the characteristic reflectance ratio of band λ and solving for $i_\lambda{}^*R_{r,\lambda}$, we obtain:

$$i_\lambda{}^*R_{r,\lambda} = (P_\lambda - C_\lambda)/(f + (1 - f)^*S_\lambda) \qquad (5)$$

We must now compute the values of the parameters S_λ and C_λ.

Assuming that the illumination factor i_λ is independent of rock and ice, pixel values corresponding to 100% rock ($f = 1$) and to 100% ice ($f = 0$) groundels can be derived from Equation (1):

$$P_{r,\lambda} = i_\lambda{}^*R_{r,\lambda} + C_\lambda$$
$$P_{i,\lambda} = i_\lambda{}^*R_{i,\lambda} + C_\lambda$$

These represent the parametric equations of straight lines in the space $(DN_{r,\lambda}, DN_{i,\lambda})$. Solving for i_λ and by substituting $S_\lambda = R_{i,\lambda}/R_{r,\lambda}$ we obtain the straight line equation:

$$P_{i,\lambda} = S_\lambda{}^*P_{r,\lambda} + (1 - S_\lambda)^*C_\lambda \qquad (6)$$

We can compute the value of S_λ by imposing the passage of this line for two known $P_{r,\lambda}$ and $P_{i,\lambda}$ pairs. In particular, we selected as pairs the mean DNs of 100% rock and 100% ice pixels in shadowed areas ($PM_{rs,\lambda}, PM_{is,\lambda}$) and in lighted ones ($PM_{rl,\lambda}, PM_{il,\lambda}$). From Equation (6) we can then compute the slope S_λ of the line and the C_λ

value:

$$S_\lambda = (PM_{is,\lambda} - PM_{il,\lambda})/(PM_{rs,\lambda} - PM_{rl,\lambda}) \qquad (7)$$

$$C_\lambda = (PM_{is,\lambda} - S_\lambda{}^*PM_{rs,\lambda})/(1 - S_\lambda) \qquad (8)$$

In conclusion, by means of (5), (8), (4) and (7) for each pixel with DN equal to P_λ we can compute
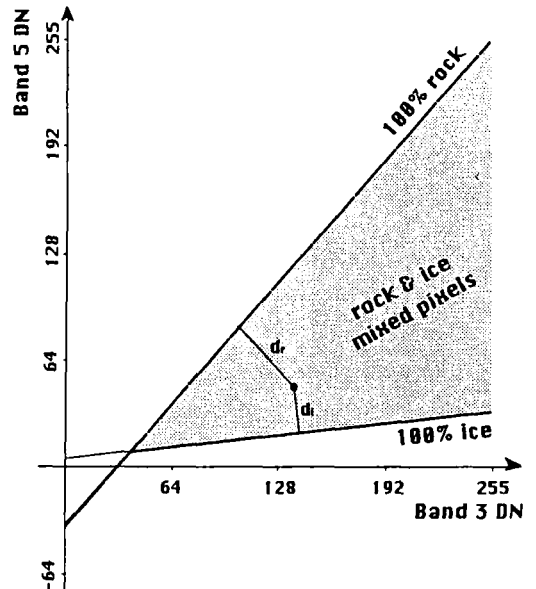

Fig. 6. Graphic showing the utilised model for recomputing the mixed pixels; the correlation lines were obtained by means of the process shown in Fig. 5. d_r and d_i represent the distances of a mixed pixel from the two correlation lines.

the value P'_λ (according to equation 2) which best expresses the information on the rock present in the groundel corresponding to that pixel. In order to reduce the effects due to non linear variations in reflectance of rock and ice categories, the recomputation process was only applied to pixels with an f value greater than a threshold f*, which in our application was conservatively established as 0.3 (30% of outcropping rock in the groundel).

This threshold was adopted in order to reduce the influence of ice in recomputing the rock spectra and to overcome the limits of the methodology. The comparison between images A and B in Fig. 7 shows that most of 10–30% rock fraction pixels apparently falls on ice covered areas.

To compute the values necessary for the whole process, we chose one test area ("Simpson Crags", test area No. 14) where the rock and ice categories are significantly represented. This area can be considered representative of the global scene as determined by a comparison of the category mean values. This is shown in Table 4 where each element is computed as:

$$a_{i,j} = ABS\{(M_{i,j} - V_{i,j})/\sigma_{i,j}\}$$

where:

$M_{i,j}$ = mean value of category i, band j (Table 1)
$V_{i,j}$ = value of category i, band j in the Simpson Crags area
$\sigma_{i,j}$ = standard deviation of category i, band j (Table 2)

We evaluated the values of the parameters related to this selected sample and then applied them to the global TM scene. The computed values of the coefficients m_r, k_r, m_i, k_i of (3) are:

$$m_r = 1.137 \quad k_r = -35.830$$
$$m_i = 0.115 \quad k_i = 4.158$$

To generate a new image where mixed pixels are replaced with new values that enhance rock information, we need first to compute the expressions (7) and (8) by making use of the mean values of pure ice pixels and of pure rock pixels. So we evaluated the mean values of 100% lighted rocks, 100% shadowed rocks, 100% lighted ice and 100% shadowed ice in the test area. These values are listed in Tables 4 and 5.

Results and discussion

The entire process, as shown in the flow chart of Fig. 2, was applied to the whole scene of the Landsat TM satellite image (date: 19/1/90, WRS: 062–113). Fig. 7A shows a significant subset of it (northern Eisenhower Range area), as an example of the final output. This image is a 4-3-2 band (R-G-B) color composite. The enhancement was obtained by using a color compensation look-up table to reduce the dominance of blue. As a side product we obtained a thematic mapping of the area, featuring as DN the rock percentage in the groundels. Fig. 7B shows a sliced partial representation of it with the same extension of the image of Fig. 7A.

The final result presented in fig 7A constitutes an enhanced image of rock information in which the number of 100% rock pixels is improved by 2.7 times. That is, the rock enhanced pixels were 1.7 times the number of pure rock pixels and they correspond to 2% of the whole image. This will produce more effective spectral classifications of rock types in further analyses of the image, and more significant reference maps for geological field-work.

The algorithm was applied by using an appro-

Table 4. Standardised mean value differences of Simpson Crags area.

	Band 1	Band 2	Band 3	Band 4	Band 5	Band 6	Band 7
a_{il}	0.04	0.93	0.80	0.95	0.76	0.01	0.75
a_{rl}	1.07	0.93	0.98	0.94	0.31	0.34	0.22
a_{is}	0.21	0.20	0.22	0.22	0.15	1.47	0.15
a_{rs}	0.42	0.39	0.46	0.50	0.07	0.42	0.19

Fig. 7. Image A: Final rock enhanced image, RGB band combination 4, 3, 2. Note the occurrence of variations in the spectra of outcropping rocks due to different lithotype (i.e. the occurrence in the centre left of the image of granites, light brown, and shales, dark brown). Image B: Outcropping rock thematic image; DNs represent the rock fraction (f) in the corresponding groundel, in percent: gray 0% < f < 10%, blue 10% < f < 20%, cyan 20% < f < 30%, green 30% < f < 50%, yellow 50% < f < 80%, red 80% < f < 100%.

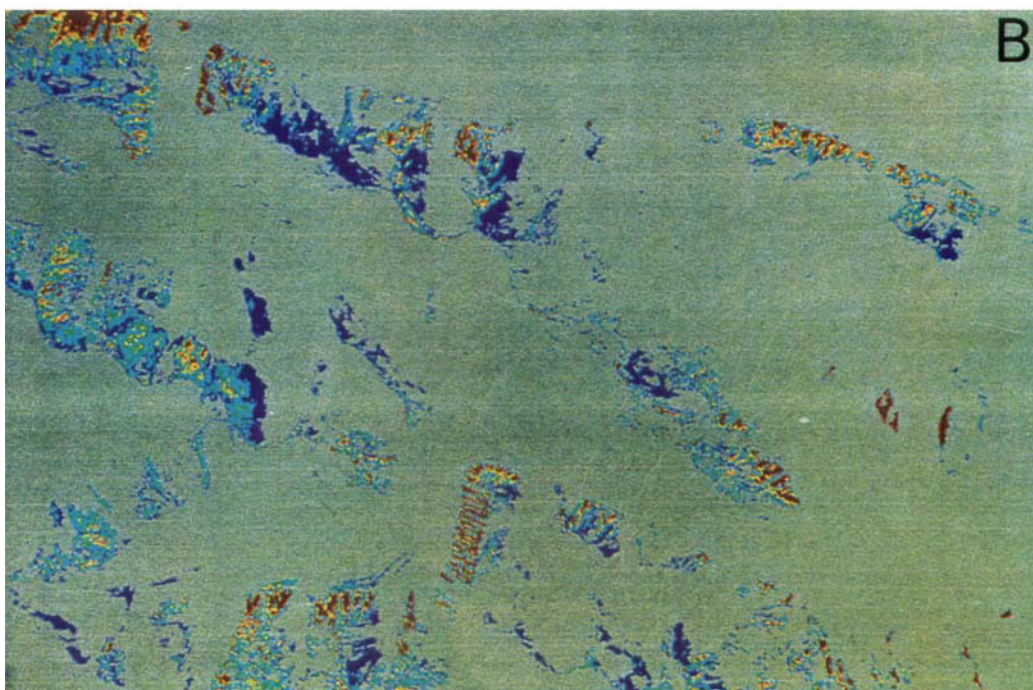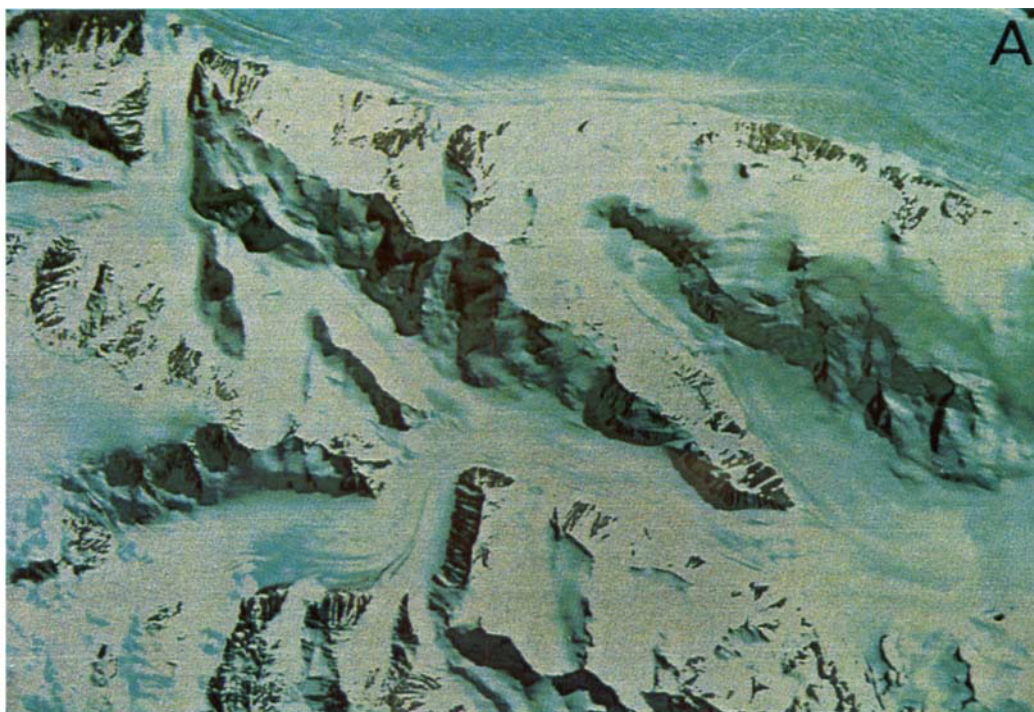*Table 5.* Mean values and standard deviations of sample subcategories in Simpson Crags area.

	Band 1	Band 2	Band 3	Band 4	Band 5	Band 6	Band 7
PM_{il}	255.00	225.33	246.75	211.57	31.43	59.24	17.26
σ	0.00	34.19	13.74	37.11	2.02	8.45	1.67
PM_{rl}	167.28	73.00	95.67	71.18	79.95	77.34	52.39
σ	29.14	15.57	22.37	18.16	22.84	9.56	14.88
PM_{is}	190.82	62.24	65.30	39.05	9.14	41.13	5.99
σ	21.12	11.12	15.28	11.29	2.85	2.56	1.72
PM_{rs}	117.26	42.00	45.70	29.63	19.14	56.25	11.31
σ	14.07	7.73	10.31	8.31	12.62	2.81	6.69

priate confidence level on computed rock fraction: the determined lower limit is 30%, under which the computation is affected by the limitation due to the discrete nature of DNs and the poor amount of information related to rock in those DNs.

The proposed algorithm constitutes an improvement in the methodology discussed by Salvini et al. (1991), for MSS images. The improvement comes from both the preparation of a more sophisticated algorithm and the possibility of using more significant intervals of the e.m. spectrum.

It is worthwhile to note that first order mathematics we developed allows the preservation of most of the variation in reflectance of the various rock types outcropping in the area (see Fig. 7A).

Fig. 8 shows that most of the variability of rock category is preserved through the enhancement. Meanwhile the number of mixed pixels is decreased and the scattered values of diagrams in Fig 8A and 8B are clustered around the rock correlation space.

Since the project was developed for a geological survey of Northern Victoria Land, the emphasis was on enhancement of rocky outcrops. However, the same algorithm could well be used to improve ice mapping in areas where DNs are affected by the presence of significant percentages of moraines and detrital in the groundels.

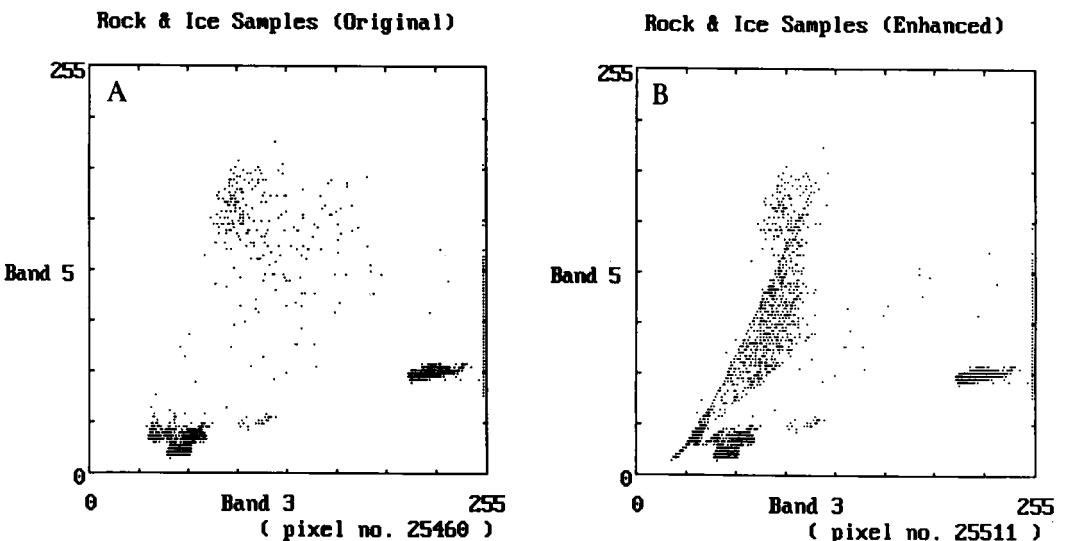Rock & Ice Samples (Original)   Rock & Ice Samples (Enhanced)

Fig. 8. Comparison between scatterograms of ice and rock samples (5,3 TM band combination) of Simpson Crags area (part of the images in Fig. 7). A, original data; B, after processing. Note the migration of mixed pixels in the rock category sector and the preservation of most of spectrum variability within the rock category.

References

Bianchi, R., Casacchia, R., Poscolieri, M., Lucchitta, B. K. & Picchiotti A. 1990: Image Processing Techniques Applied to Landsat MSS Images of Victoria Land, Antarctica. *Mem. Soc. Geol. It.* 43, 155–163 (1988).

Bianchi, R., Casacchia, R., Poscolieri, M. & Picchiotti, A. 1991: Digital Enhancement Techniques applied to Landsat MSS Images of Victoria Land, Antarctica. *Mem. Soc. Geol. It.* 46, 525 (1989).

Bierwirth, P. N. 1990: Mineral mapping and vegetation removal via data-calibrated pixel unmixing, using multispectral images. *Int. J. Remote Sensing*, Vol. 11(11), 1999–2017.

Borfecchia, F. & Frezzotti, M. 1991: Satellite Image Mosaic of the Terra Nova Bay Area (Victoria Land, Antarctica). *Mem. Soc. Geol. It.* 46, 521–523 (1989).

Carmignani, L., Ghezzo, C., Gosso, G., Lombardo, B., Meccheri, M., Montrasio, A., Pertusati, P. C. & Salvini, F. 1989a: Geological Map of the Area Between David and Mariner Glaciers, Victoria Land – Antarctica. *Mem. Soc. Geol. It.* 33, (1987).

Carmignani, L., Ghezzo, C., Gosso, G., Lombardo, B., Meccheri, M., Montrasio, A., Pertusati, P. C. & Salvini, F. 1989b: Geology of the Wilson Terrane in the area between David and Mariner Glaciers, Victoria Land (Antarctica). *Mem. Soc. Geol. It.* 33 77–97 (1987).

Fortunati, L., della Maggiore, R., Mazzarini, F., Salvini, F. & Spano', M. 1991: Regional scale structural geology of Northern Victoria Land (Antarctica) by satellite image processing. *Mem. Soc. Geol. It.* 46, 495–504 (1989).

Gair, H. S., Sturm, A., Carryer, S. J. & Grindley, G. W. 1969: The Geology of Northern Victoria Land. *Am. Geogr. Soc. Antarctic Map Folio Series*, Folio 12, Plate XII.

Ganovex Team 1987: Geological Map of the North Victoria Land, Antarctica (1 : 500,000). Explanation Notes. *Geol. Jb.* B66: Hannover, 7–79.

Giudice, A., Mazzarini, F., Salvini, F. & Storti, F. 1991a: Geology of the Mt. Melbourne area, North Victoria Land, Antarctica: Evidence from Photointerpretative analysis. *Mem. Soc. Geol. It.* 46, 505–514 (1989).

Giudice, A., Mazzarini, F., Salvini, F. & Storti, F. 1991b: Geological map at 1 : 100,000 scale of Mt. Dickason and Mt. Levick areas, North Victoria Land, Antarctica. *Mem. Soc. Geol. It.* 46, (1989).

Kleinshmidt, G., Roland, N. W. & Schubert, W. 1984: The Metamorphic Basement Complex in the Mountaineer Range, North Victoria Land (Antarctica). *Geol. Jb.* B 60, 213–251.

Lucchitta, B. K., Bowell, J. A., Edwards, K., Eliason, E. M. & Ferguson, H. M. 1987: Multispectral Landsat Images of Antarctica. *U.S. Geological Survey Bulletin*, 1696. 21 pp.

Lucchitta, B. K., Bowell, J. A. & Tessensohn, F. 1989: Landsat Image for Antarctic Research. *Mem. Soc. Geol. It.* 33, 35–40 (1987).

Orombelli, G. 1989: Terra Nova Bay: a Geographic Overview. *Mem. Soc. Geol. It.* 33, 69–75 (1987).

Salvini, F., Mazzarini, F., Fortunati, L., della Maggiore, R. & Mogorovich, P. 1991: Rock-enhanced thematic mapping of glaciated terranes from satellite imagery in Antarctica. *Mem. Soc. Geol. It.* 46, 515–520 (1989).

Wadge, G. & Quarmby, N. 1988: Geological remote sensing of rocky coasts. *Geol. Mag.* 125(5), 495–505.

Wise, D. U., Funiciello, R., Parotto M., & Salvini, F. 1985: Topographic lineament swarms: clues to their origin from domain analysis of Italy. *Geol. Soc. of Am. Bull.* 96, 952–967.